AGU PUBLICATIONS

Geophysical Research Letters

RESEARCH LETTER
10.1002/2015GL063956

Key Points:
- First millennial climate reconstruction based on extratropical tree ring density network
- Improved ratio between low- and high-frequency temperature variability
- New insights into postvolcanic cooling and the onset of the Little Ice Age

Supporting Information:
- Text S1, Figures S1–S11, and Tables S1 and S2

Correspondence to:
L. Schneider,
l.schneider@geo.uni-mainz.de

Citation:
Schneider, L., J. E. Smerdon, U. Büntgen, R. J. S. Wilson, V. S. Myglan, A. V. Kirdyanov, and J. Esper (2015), Revising midlatitude summer temperatures back to A.D. 600 based on a wood density network, *Geophys. Res. Lett.*, *42*, doi:10.1002/2015GL063956.

Received 23 MAR 2015
Accepted 14 MAY 2015
Accepted article online 18 MAY 2015

Revising midlatitude summer temperatures back to A.D. 600 based on a wood density network

Lea Schneider[1], Jason E. Smerdon[2], Ulf Büntgen[3], Rob J. S. Wilson[2,4], Vladimir S. Myglan[5], Alexander V. Kirdyanov[6], and Jan Esper[1]

[1]Department of Geography, Johannes Gutenberg University, Mainz, Germany, [2]Lamont-Doherty Earth Observatory of Columbia University, Palisades, New York, USA, [3]Swiss Federal Research Institute WSL, Birmensdorf, Switzerland, [4]School of Geography and Geosciences, University of St Andrews, St Andrews, UK, [5]Institute for the Humanities, Siberian Federal University, Krasnoyarsk, Russia, [6]V.N. Sukachev Institute of Forest SB RAS, Krasnoyarsk, Russia

Abstract Annually resolved and millennium-long reconstructions of large-scale temperature variability are primarily composed of tree ring width (TRW) chronologies. Changes in ring width, however, have recently been shown to bias the ratio between low- and high-frequency signals. To overcome limitations in capturing the full spectrum of past temperature variability, we present a network of 15 maximum latewood density (MXD) chronologies distributed across the Northern Hemisphere extratropics. Independent subsets of continental-scale records consistently reveal high MXD before 1580 and after 1910, with below average values between these periods. Reconstructed extratropical summer temperatures reflect not only these long-term trends but also distinct cooling pulses after large volcanic eruptions. In contrast to TRW-dominated reconstructions, this MXD-based record indicates a delayed onset of the Little Ice Age by almost two centuries. The reduced memory inherent in MXD is likely responsible for the rapid recovery from volcanic-induced cooling in the fourteenth century and the continuation of warmer temperatures until ~1600.

1. Introduction

Integration of climate proxies and development of continental-scale temperature reconstructions of the past millennium has greatly improved our understanding of the spatial patterns of long-term climate variability [*PAGES 2k Consortium*, 2013]. It has been shown [*Bunde et al*., 2013; *Franke et al*., 2013], however, that the spectral characteristics of temperature fluctuations in proxy-based reconstructions differ systematically from observations, with the proxies overestimating the ratio of low- to high-frequency variability. This "red bias" [*Franke et al*., 2013] inherent to reconstruction spectra is a fundamental constraint limiting the assessment of preinstrumental climatic extremes [*Anchukaitis et al*., 2012; *D'Arrigo et al*., 2013; *Esper et al*., 2013], which in turn has implications for the estimation of the Earth's climate sensitivity through comparisons of climate model simulations with proxy-based reconstructions of preindustrial temperature variability [*Frank et al*., 2010].

Almost all millennial-scale temperature reconstructions assessed in the Intergovernmental Panel on Climate Change Fifth Assessment Report (IPCC AR5) [*Masson-Delmotte et al*., 2013] are either solely based on tree ring data or a combination of these data with multiple additional proxies—most of which have lower temporal resolution. The interannual variance in these records is nevertheless dominated by tree ring width (TRW) measurements, a parameter known to contain substantial biological memory [*Frank and Esper*, 2005] due to the persistence of needle generations and storage of reserves throughout dormancy [*Fritts*, 1976]. These effects translate into an overestimation of the persistence of postvolcanic temperature cooling [*Frank et al*., 2007a; *Masson-Delmotte et al*., 2013] and biased spectral characterization of tree ring-based temperature reconstructions [*Bunde et al*., 2013; *Franke et al*., 2013]. Maximum latewood density (MXD), in contrast, has the capacity to more directly respond to and recover from pulse-like cooling [*Briffa et al*., 1998] and disturbance [*Esper et al*., 2007a] events. Less physiological noise results in a stronger common signal among trees and stronger coherence between observational target and proxy data [*Esper et al*., 2013]. Moreover, compared to TRW, the relative magnitude of biologic age trends in MXD is smaller with respect to the standard deviation of the samples, therefore reducing the distortion effects that arise during the necessary process of detrending, which again supports the fidelity of millennial-scale temperature

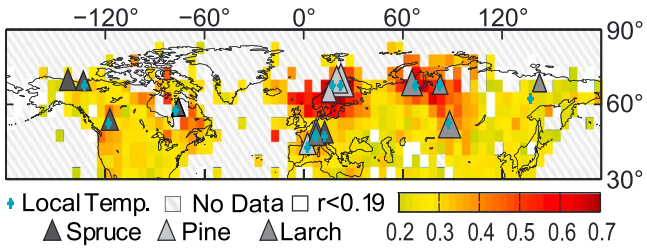

Figure 1. June-July-August temperature correlation field represented by NH extratropical tree ring density records. The MXD data collection (triangles) comprises temperature sensitive pine, larch, and spruce site chronologies. The size of the triangles represents the length of the chronologies (637–2187 years). Colors indicate the average Pearson's correlation coefficient of all statistically significant ($p < 0.05$, one sided) correlations between the MXD chronologies and gridded observational temperatures from 1901 to 1976. White cells indicate areas not (significantly) represented by any MXD chronology, and blue stars mark the grid cells used for local weighting and pseudoproxy experiments.

variance estimated from this parameter [*Esper et al.*, 2012]. Nevertheless, a large-scale compilation of the longest MXD chronologies has not yet been used to estimate hemispheric-scale high- to low-frequency variability in temperature over the last millennium.

We introduce herein a network of the 15 longest available MXD records (Table S1 in the supporting information) from Asia, Europe, and North America (4/7/4), assess the climate signal inherent in these data, and develop an alternative Northern Hemisphere (NH) reconstruction. The proxy network comprises in total less site chronologies than the most recent TRW-based reconstruction [*D'Arrigo et al.*, 2006] but is similarly replicated at the onset of the last millennium. Excluding TRW from our evaluations allows us to assess the potential benefits of a parameter free of biological memory effects and its ability to theoretically overcome the spectral limitation associated with TRW-derived estimates.

2. Data and Methods

2.1. Proxy Network

Proxy data for this study are publicly available at the International Tree Ring Data Bank or contributed by the original authors [*Anchukaitis et al.*, 2013; *Briffa et al.*, 2013; *Büntgen et al.*, 2006, 2008; *Esper et al.*, 2007b, 2012; *Luckman and Wilson*, 2005; *Melvin et al.*, 2013; *Myglan et al.*, 2012; *Schweingruber et al.*, 1988]. All data sets were corrected separately for biological and site-related noise using regional curve standardization (RCS) [*Briffa et al.*, 1992; *Esper et al.*, 2003]. Residuals between the power-transformed [*Cook and Peters*, 1997] MXD series and an expected age-related growth curve were calculated and averaged using the robust biweight mean to form site chronologies. Tree ring data from Athabasca and Mangazia comprised site- or species-specific offsets in the mean growth level. These sites were divided into subgroups, according to species composition and growth rate, detrended separately using RCS, and recombined to form mean site chronologies (Text S1) [*Luckman and Wilson*, 2005].

The varying sample replication of the single site chronologies necessitates variance stabilization, here achieved by fitting a 100 year spline through the absolute departure values and dividing the chronologies by this spline curve. Other plausible tree ring standardization methods (e.g., signal-free detrending or replication-based variance correction) were also tested, yielding similar results (Figure S1 and Table S2). Fifteen detrended site chronologies longer than 600 years and replicated with at least three samples served as the final predictor network (Figure 1 and Table S1). The shortest record starts in 1363 and the oldest terminates in 1976, the last year of the calibration period. All records passed a benchmarking experiment evaluating the strength of local June-July-August (JJA) temperature responses via a random process. A 95% confidence level is derived from the probability distribution of correlations between local temperature and 1000 red noise time series with first-order autocorrelation matching each MXD record. Local correlations between each MXD chronology and temperature served as the weights in the hemispheric composites used in the reconstruction procedure. Records from the Alps and Scandinavia were averaged to regional composites to mitigate the European sampling bias.

2.2. Instrumental Target

The instrumental target is monthly mean JJA temperature derived from the $5 \times 5°$ CRUTEM4v network (30°–90°) [*Jones et al.*, 2012]. The field was truncated in 1901, due to an increasing number of empty grid cells (53% at the onset of the twentieth century and 86% in 1850) and subsequent variance

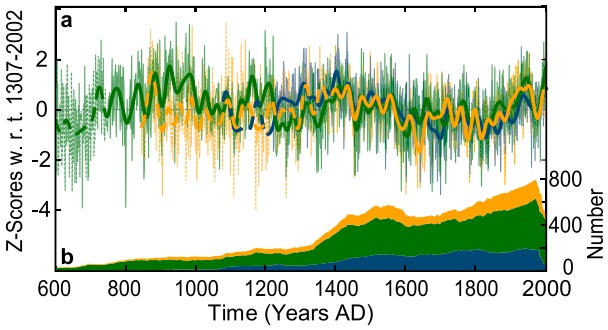

Figure 2. Continental MXD chronologies. (a) Continental-scale MXD compilations derived from four site chronologies in North America (blue), seven chronologies in Europe (green), and four chronologies in Asia (yellow). Thick curves are filtered reconstructions using a 30 year low-pass butterworth filter. Continental averages with less than three sites are dashed. (b) The overall number of samples by continent.

reduction in the NH mean due to the gap filling via the regularized expectation maximization algorithm using ridge regression [*Schneider*, 2001]. Regional and hemispheric temperature averages were weighted by area, using the cosine latitude of local grid cell centers. For analyses of growth responses, we chose CRUTEM4v temperatures from the grid cell containing the corresponding tree site. Cells with very short records were replaced by records from neighboring cells (e.g., in eastern Siberia; Figure 1). Monthly averaged diurnal temperature maxima for JJA, tested as an alternative instrumental target [*Wilson et al.*, 2007], yielded neither consistent nor significant improvements in the calibration results.

2.3. Calibration/Validation

The regional MXD chronologies were combined into an ensemble estimate of hemispheric temperature variability by calculating weighted composites based on moving correlations with local temperature. The composite averages were scaled against NH extratropical temperatures over the 1901–1976 period [*von Storch et al.*, 2009]. Calibration and validation statistics (R^2 and RE metrics [*Briffa et al.*, 1988]) were estimated using a 38 year holdout window incremented by 1 year between 1901 and 1976 to derive an ensemble of 76 plausible reconstruction members (Figure S2). The procedure enabled the estimation of a calibration error derived from minimum and maximum reconstructed temperatures for each year. The decreasing number of predictors back in time, typical for dendroclimatological studies, results in increasing uncertainty in earlier periods, which was accounted for by recalculating the reconstruction and associated errors each time a site record dropped out (Figure S3) [*Cook et al.*, 2002]. Such a nested approach also allowed the variance to be adjusted to account for the diminishing predictor network, as well as validation metrics and sampling error estimates to vary in time. Artificial reduction of site-specific replication by randomly drawing from all MXD series in the twentieth century revealed only negligible differences in estimated errors (Figure S4). Moreover, the sensitivity of the reconstruction against a changing predictor network and different calibration choices was assessed (Figures S5 and S6). The recent end of the proxy network is characterized by a quickly declining number of sites. The 1976–2002 period was thus reconstructed with only one nest containing seven records extending into the 21st century.

3. Results

The MXD network has reasonable coverage over the last millennium with all data sets reaching back to A.D. 1363. Each chronology explains a significant fraction of regional summer temperature variability, verified in a benchmarking experiment, and the combined correlation fields ($p < 0.05$) from all records represent 90% of the NH extratropical landmass (Figure 1). In addition to validating the MXD data against local observations and regional temperature fields, the combined site chronologies display strong coherence at continental (North America, Europe, and Asia) scales (Figure 2). The explained variance among 30 year low pass-filtered continental means over the common A.D. 1363–1976 period is $\overline{R}^2_{1363-1976} = 0.45$ ($R^2_{\text{America/Asia}} = 0.47$, $R^2_{\text{America/Europe}} = 0.40$, and $R^2_{\text{Asia/Europe}} = 0.49$) indicating sensitivity to common forcing and/or modes of variability at multidecadal to centennial timescales. The correlation coefficients decline during the early, less replicated portion of the records. At interannual timescales there is no coherence between the continental composite ($\overline{R}^2_{1363-1976} = 0.03$), corresponding to the reduced spatial coherency of surface temperature fields in the higher-frequency domain [*Jones et al.*, 2012].

The large-scale reconstruction correlates (Pearson's r) at $r_{1901-1976} = 0.60$ with modern JJA temperatures and estimates preinstrumental temperatures to have spanned 0.54 ± 0.34°C between the coldest 30 year periods during the Little Ice Age (LIA) (1627–1656 and 1809–1838) and the warmest such period during late medieval

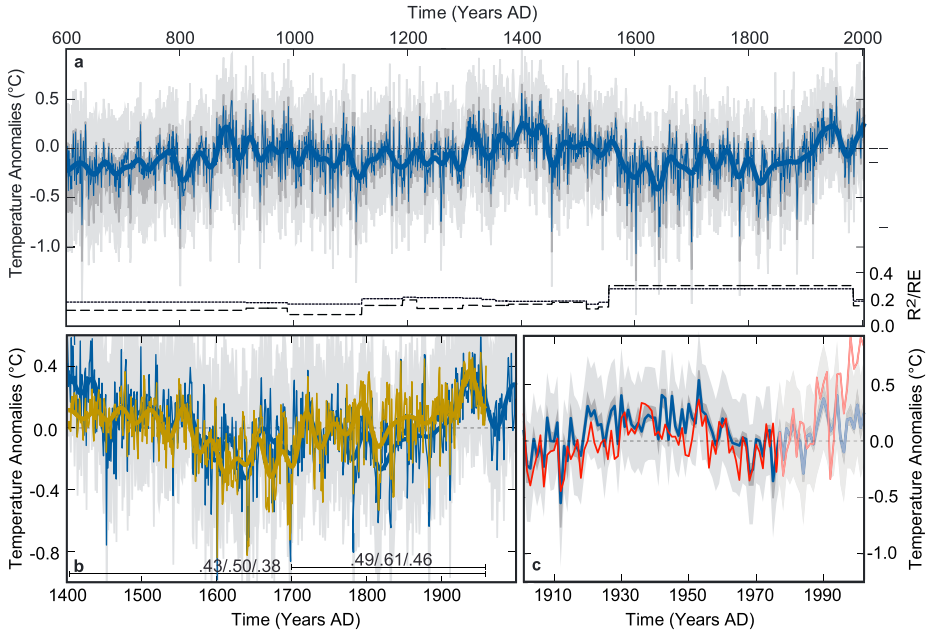

Figure 3. NH extratropical temperature reconstruction. (a) Nested June-July-August temperature reconstruction (blue) with combined uncertainty estimates derived from the calibration (dark grey) and sampling (light grey) errors. Anomalies with respect to 1961–1990. Bottom panel shows the time-varying explained variance (R^2; dotted) and reduction of error statistic (RE; dashed) of differently replicated nests over the past 1400 years. All nests passed the 99% threshold of a red noise benchmarking exercise (see Text S1). (b) MXD-based temperature reconstructions from this study (blue) and reference [*Briffa et al.*, 2001] (brown) as anomalies with respect to 1402–1960. Values at the bottom are explained variances (R^2) between the actual, low pass-filtered, and high pass-filtered records (the latter is not shown graphically). (c) The MXD-based reconstruction as in Figure 3a (blue) together with instrumental JJA temperatures averaged over the NH extratropics (red) during the 1901–1976 period common to all predictors. The less replicated most recent decades are shown in faded colors. Anomalies with respect to 1961–1990.

times (1396–1425) (Figure 3). The same temperature range is reconstructed from the LIA to the warmest most recent 30 year period (1927–1956). The reconstruction indicates moderate summer temperatures from ~ A. D. 900 to 1600 at the hemispheric scale, with maxima occurring in the late ninth and midfifteenth centuries, followed by cooler summers from ~ 1600 to 1900 and subsequent twentieth century warming.

The new summer temperature reconstruction was validated using stepwise ensemble techniques, a sliding calibration/verification approach and pseudoproxy experiments (Text S1 and Figures S2, S3, and S7; see *Smerdon* [2012] for a review). Despite considerable empirical uncertainty, the reconstruction proved robust to a number of methodological choices during calibration (Figures S6a–S6h). Potential divergence issues [*Esper et al.*, 2010; *Wilson et al.*, 2007], which become apparent in some of the local records in the late twentieth century, were evaluated by compiling two independent records derived from eight "nondiverging" and five "diverging" MXD site chronologies (Figures S8–S10). Despite low site replication, both subsamples share a considerable amount of low-frequency variability in their common period (1363–1976) followed by a more significant offset in the late twentieth century. In the complete composite, decoupling between the instrumental and proxy-derived temperatures is noted in the most recent decades. The new JJA temperature reconstruction also coheres closely with a shorter reconstruction based on 300+ MXD sites distributed over the NH extratropics, the so-called "Schweingruber MXD network" [*Briffa et al.*, 2001] (Figure 3b). These two almost independent data sets (estimated data overlap $< 1\%$) correlate at $r = 0.70$ over the past ~300 years. An offset of ~0.2°C evolving before 1450 is likely related to the changing spatial coverage in the Schweingruber network, while sample and site replication remain stable during this period in our new network of long MXD records.

4. Discussion and Conclusion

Comparison of the new MXD-based reconstruction with the multiproxy and TRW-based records assessed by the IPCC [*Masson-Delmotte et al.*, 2013] reveals substantial differences at low and high frequencies (Figure 4).

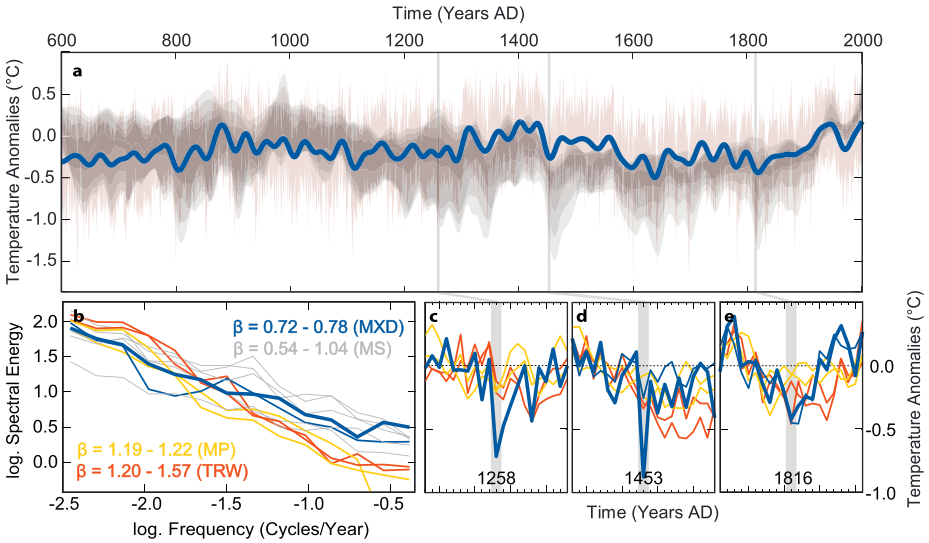

Figure 4. Comparison of Northern Hemispheric temperature reconstructions. (a) This study (blue) shown together with the distribution quantiles (grey shading) derived from 15 reconstructions assessed in the IPCC AR5 [*Masson-Delmotte et al*., 2013] after 30 year low pass filtering. Note that most reconstructions are scaled to annual mean temperature. Anomalies with respect to 1901–1976. Grey bars indicate major volcanic eruptions. (b) Spectral energy and β values for this study (bold blue), the MXD-based reconstruction from *Briffa et al*. [2001] (thin blue), two TRW-based reconstructions (red) [*D'Arrigo et al*., 2006; *Frank et al*., 2007b], two multiproxy-based reconstructions (MP) (yellow) [*Moberg et al*., 2005; *Juckes et al*., 2007], and five model simulations (grey, MS). Mean and variance are adjusted over the 1923–1960 period in the time domain, representing the common period during the calibration interval. (c–e) Temperature anomalies following the volcanic eruptions in 1257, 1452, and 1815 with respect to 10 preceding years. Colors are as in Figure 4b.

Modern warming is poorly represented in the new record questioning the ability of MXD to capture very warm temperatures. The last several decades of the reconstruction are, however, represented by a smaller number of chronologies. Among these, only a couple appears to be impacted by divergence, suggesting deficiencies regarding spatial representation or chronology quality, rather than a whole-scale limitation of the proxy. While the overall sequence of warmer conditions during medieval times, subsequent LIA cooling, and twentieth century warming is in accordance with the IPCC collection of reconstructions, the new record deviates substantially regarding the initiation of the LIA and the millennial-scale temperature amplitude. The Medieval Warm Period is less pronounced in our reconstruction, and summer temperatures remain at a relatively warm level throughout the ~1300–1450 period, when the existing reconstructions indicate a prolonged cooling trend. Residuals are largest in the late fifteenth and sixteenth centuries during which the MXD-based estimates point to warmer conditions, thereby delaying the onset of the LIA until the early seventeenth century—a substantial change important to the discussion about potential drivers of NH cooling [*Schurer et al*., 2014] and the interpretation of potential societal responses [*Büntgen et al*., 2011].

Some of these differences possibly arise as a result of varying seasonal or spatial coverage. Although most of the reconstructions in the IPCC ensemble are likely biased toward a summer signal, many of them target annual temperatures. For TRW-based reconstructions, this assumption is ascribed to the longer season portrayed by ring width due to biological-driven persistence [*D'Arrigo et al*., 2006; *Frank et al*., 2007a]. Thus, the more confined seasonal fingerprint of MXD could explain deviations to some extent. Other studies, in contrast, state that multidecadal variability should be largely independent of the season chosen [*Cook et al*., 2004], and we find some evidence for that at least during the observational period (Figures S6i and S6j). By focusing strictly on long MXD records, this reconstruction has a reduced spatial coverage during the calibration period compared to the most recent tree ring-based reconstruction [*D'Arrigo et al*., 2006]. Coherency with observational data is nevertheless good in the middle- and low-frequency domains and does not imply discrimination based on the network extent (Figure S11). Despite these findings, it is also clear that spatially expanding the extent of the NH MXD network would greatly benefit future paleoclimatological research.

A remaining rationale for deviating long-term trends and the delayed LIA onset likely originates from the different response of MXD data, compared to TRW, to a cluster of major volcanic eruptions in the thirteenth and subsequent centuries (compared to the relative lack of such events during medieval times) as revealed in Greenland and Antarctic ice core data [*Gao et al*., 2008]. For the TRW and multiproxy reconstructions, spectral power is shifted from annual and multidecadal timescales to lower frequencies, compared to the model simulations and MXD reconstruction, which indicates prolonged responses to climate variations in the traditional data (Figure 4b and Text S1). At the large spatial scale addressed here, these differences become visible during the periods subsequent to the three largest volcanic eruptions of the past millennium in 1257, 1452, and 1815 (Figures 4c–4e). Whereas the TRW-dominated reconstructions show a weak and temporally extended postvolcanic response, the MXD-based reconstructions reveal distinct postvolcanic cooling and recover to mean climatology much faster. Of particular interest is the temperature drop after the 1257 event, recorded in ice cores, providing further evidence for the precise dating of tree ring records over the entire millennium [*Anchukaitis et al*., 2012]. The MXD-based reconstruction from *Briffa et al*. [2001] indicates less cooling after the 1452 event, most likely related to decreased spatial replication in the earliest part of this record. Cooling in response to Tambora (1815) is less distinct as it coincides with the generally cold Dalton Minimum (~1790–1830) [*Wagner and Zorita*, 2005].

Model-simulated temperatures support the fast recovery from volcanic-induced cooling [*Wigley et al*., 2005] as recorded in the MXD-based reconstruction, although some models reveal a much stronger—and potentially too strong—temperature response [*Landrum et al*., 2013]. The temperature trend from the Medieval Warm Period into the LIA also appears reduced in some model simulations [*Fernández-Donado et al*., 2013]. It remains unclear, however, whether this is due to less persistent volcanic cooling, an underestimation of internal variability, or the influence of solar variability. Considering the differing spectral characteristics identified herein (Figure 4b), and confirmed by *Bunde et al*. [2013] and *Franke et al*. [2013], it seems important that our new MXD-based reconstruction has similar spectral properties to the simulated temperatures at frequencies ranging from 0.5 to 0.003 cycles per year. Although millennium-long oscillations are poorly sampled, our calculated beta values indicate that the new temperature history is not red biased, as is typical for the TRW and multiproxy reconstructions. Consideration of the new reconstruction might thus strengthen efforts to estimate the climate sensitivity to volcanic eruptions and the persistence of subsequent lower tropospheric cooling. The late initiation of the LIA around 1580 revealed in our reconstruction might additionally help to further elucidate ecosystem responses and historical linkages throughout the past millennium.

Acknowledgments
We thank all of our colleagues for developing millennial-length MXD chronologies and making these data available. This study was supported by the Mainz Geocycles Research Centre. Supplementary information is available in the online version of the paper. Data are available via the NOAA online server. Lamont contribution 7902.

The Editor thanks two anonymous reviewers for their assistance in evaluating this paper.

References

Anchukaitis, K. J., et al. (2012), Tree rings and volcanic cooling, *Nat. Geosci.*, *5*(12), 836–837.
Anchukaitis, K. J., R. D'Arrigo, L. Andreu-Hayles, D. Frank, A. Verstege, A. Curtis, B. M. Buckley, G. C. Jacoby, and E. R. Cook (2013), Tree-ring-reconstructed summer temperatures from northwestern North America during the last nine centuries, *J. Clim.*, *26*(10), 3001–3012.
Briffa, K. R., P. D. Jones, J. R. Pilcher, and M. K. Hughes (1988), Reconstructing summer temperatures in northern Fennoscandinavia back to A.D. 1700 using tree-ring data from Scots pine, *Arct. Alp. Res.*, *20*(4), 385–394.
Briffa, K. R., P. D. Jones, T. S. Bartholin, D. Eckstein, F. H. Schweingruber, W. Karlén, P. Zetterberg, and M. Eronen (1992), Fennoscandian summers from A.D. 500: Temperature changes on short and long timescales, *Clim. Dyn.*, *7*(3), 111–119.
Briffa, K. R., P. D. Jones, F. H. Schweingruber, and T. J. Osborn (1998), Influence of volcanic eruptions on Northern Hemisphere summer temperature over the past 600 years, *Nature*, *393*(6684), 450–455.
Briffa, K. R., T. J. Osborn, F. H. Schweingruber, I. C. Harris, P. D. Jones, S. G. Shiyatov, and E. A. Vaganov (2001), Low-frequency temperature variations from a northern tree ring density network, *J. Geophys. Res.*, *106*, 2929–2941, doi:10.1029/2000JD900617.
Briffa, K. R., T. M. Melvin, T. J. Osborn, R. M. Hantemirov, A. V. Kirdyanov, V. S. Mazepa, S. G. Shiyatov, and J. Esper (2013), Reassessing the evidence for tree-growth and inferred temperature change during the Common Era in Yamalia, northwest Siberia, *Quat. Sci. Rev.*, *72*, 83–107.
Bunde, A., U. Büntgen, J. Ludescher, J. Luterbacher, and H. von Storch (2013), Is there memory in precipitation?, *Nat. Clim. Change*, *3*(3), 174–175.
Büntgen, U., D. Frank, D. Nievergelt, and J. Esper (2006), Summer temperature variations in the European Alps, A.D. 755–2004, *J. Clim.*, *19*(21), 5606–5623.
Büntgen, U., D. Frank, H. Grudd, and J. Esper (2008), Long-term summer temperature variations in the Pyrenees, *Clim. Dyn.*, *31*(6), 615–631.
Büntgen, U., et al. (2011), 2500 years of European climate variability and human susceptibility, *Science*, *331*(6017), 578–582.
Cook, E. R., and K. Peters (1997), Calculating unbiased tree-ring indices for the study of climatic and environmental change, *Holocene*, *7*(3), 361–370.
Cook, E. R., R. D'Arrigo, and M. E. Mann (2002), A well-verified, multiproxy reconstruction of the winter North Atlantic Oscillation index since A.D. 1400, *J. Clim.*, *15*(13), 1754–1764.
Cook, E. R., J. Esper, and R. D'Arrigo (2004), Extra-tropical Northern Hemisphere temperature variability over the past 1000 years, *Quat. Sci. Rev.*, *23*, 2063–2074.
D'Arrigo, R., R. Wilson, and G. Jacoby (2006), On the long-term context for late twentieth century warming, *J. Geophys. Res.*, *111*, D03103, doi:10.1029/2005JD006352.

D'Arrigo, R., R. Wilson, and K. J. Anchukaitis (2013), Volcanic cooling signal in tree ring temperature records for the past millennium, *J. Geophys. Res. Atmos.*, *118*, 9000–9010, doi:10.1002/jgrd.50692.
Esper, J., E. R. Cook, P. J. Krusic, K. Peters, and F. H. Schweingruber (2003), Tests of the RCS method for preserving low-frequency variability in long tree-ring chronologies, *Tree-Ring Res.*, *59*(2), 81–98.
Esper, J., U. Büntgen, D. Frank, D. Nievergelt, and A. Liebhold (2007a), 1200 years of regular outbreaks in alpine insects, *Proc. R. Soc. B*, *274*(1610), 671–679.
Esper, J., U. Büntgen, D. Frank, T. Pichler, and K. Nicolussi (2007b), Updating the Tyrol tree-ring dataset, in *Tree Rings in Archaeology, Climatology and Ecology, TRACE*, edited by K. Haneca et al., pp. 80–85, Forschungszentrum Jülich GmbH, Jülich, Germany.
Esper, J., D. Frank, U. Büntgen, A. Verstege, R. M. Hantemirov, and A. V. Kirdyanov (2010), Trends and uncertainties in Siberian indicators of 20th century warming, *Global Change Biol.*, *16*(1), 386–398.
Esper, J., et al. (2012), Orbital forcing of tree-ring data, *Nat. Clim. Change*, *2*(12), 862–866.
Esper, J., L. Schneider, P. J. Krusic, J. Luterbacher, U. Büntgen, M. Timonen, F. Sirocko, and E. Zorita (2013), European summer temperature response to annually dated volcanic eruptions over the past nine centuries, *Bull. Volcanol.*, *75*(7), 736.
Fernández-Donado, L., et al. (2013), Large-scale temperature response to external forcing in simulations and reconstructions of the last millennium, *Clim. Past*, *9*, 393–421.
Frank, D., and J. Esper (2005), Characterization and climate response patterns of a high-elevation, multi-species tree-ring network in the European Alps, *Dendrochronologia*, *22*(2), 107–121.
Frank, D., U. Büntgen, R. Böhm, M. Maugeri, and J. Esper (2007a), Warmer early instrumental measurements versus colder reconstructed temperatures: Shooting at a moving target, *Quat. Sci. Rev.*, *26*(25–28), 3298–3310.
Frank, D., J. Esper, and E. R. Cook (2007b), Adjustment for proxy number and coherence in a large-scale temperature reconstruction, *Geophys. Res. Lett.*, *34*, L16709, doi:10.1029/2007GL030571.
Frank, D., J. Esper, C. C. Raible, U. Büntgen, V. Trouet, B. Stocker, and F. Joos (2010), Ensemble reconstruction constraints on the global carbon cycle sensitivity to climate, *Nature*, *463*, 527–530.
Franke, J., D. Frank, C. C. Raible, J. Esper, and S. Brönnimann (2013), Spectral biases in tree-ring climate proxies, *Nat. Clim. Change*, *3*(4), 360–364.
Fritts, H. C. (1976), *Tree Rings and Climate*, Academic Press, London, New York.
Gao, C., A. Robock, and C. Ammann (2008), Volcanic forcing of climate over the past 1500 years: An improved ice core-based index for climate models, *J. Geophys. Res.*, *113*, D23111, doi:10.1029/2008JD010239.
Jones, P. D., D. H. Lister, T. J. Osborn, C. Harpham, M. Salmon, and C. P. Morice (2012), Hemispheric and large-scale land-surface air temperature variations: An extensive revision and an update to 2010, *J. Geophys. Res.*, *117*, D05127, doi:10.1029/2011JD017139.
Juckes, M. N., M. R. Allen, K. R. Briffa, J. Esper, G. C. Hegerl, A. Moberg, T. J. Osborn, and S. L. Weber (2007), Millennial temperature reconstruction intercomparison and evaluation, *Clim. Past*, *3*(4), 591–609.
Landrum, L., B. L. Otto-Bliesner, E. R. Wahl, A. Conley, P. J. Lawrence, N. Rosenbloom, and H. Teng (2013), Last millennium climate and its variability in CCSM4, *J. Clim.*, *26*(4), 1085–1111.
Luckman, B. H., and R. J. S. Wilson (2005), Summer temperatures in the Canadian Rockies during the last millennium: A revised record, *Clim. Dyn.*, *24*(2–3), 131–144.
Masson-Delmotte, V., et al. (2013), Information from paleoclimate archives, in *Climate Change 2013: The Physical Science Basis. Contribution of Working Group I to the Fifth Assessment Report of the Intergovernmental Panel on Climate Change*, edited by T. F. Stocker et al., pp. 383–464, Cambridge Univ. Press, Cambridge, U. K., and New York.
Melvin, T. M., H. Grudd, and K. R. Briffa (2013), Potential bias in "updating" tree-ring chronologies using regional curve standardisation: Re-processing 1500 years of Torneträsk density and ring-width data, *Holocene*, *23*(3), 364–373.
Moberg, A., D. M. Sonechkin, K. Holmgren, N. M. Datsenko, and W. Karlen (2005), Highly variable Northern Hemisphere temperatures reconstructed from low- and high-resolution proxy data, *Nature*, *433*(7026), 613–617.
Myglan, V. S., O. C. Oidupaa, and E. A. Vaganov (2012), A 2367-year tree-ring chronology for the Altai–Sayan region (Mongun-Taiga Mountain Massif), *Archaeol. Ethnol. Anthropol. Eurasia*, *40*(3), 76–83.
PAGES 2k Consortium (2013), Continental-scale temperature variability during the past two millennia, *Nat. Geosci.*, *6*(5), 339–346.
Schneider, T. (2001), Analysis of incomplete climate data: Estimation of mean values and covariance matrices and imputation of missing values, *J. Clim.*, *14*(5), 853–871.
Schurer, A. P., S. F. B. Tett, and G. C. Hegerl (2014), Small influence of solar variability on climate over the past millennium, *Nat. Geosci.*, *7*(2), 104–108.
Schweingruber, F. H., T. Bartholin, E. Schar, and K. R. Briffa (1988), Radiodensitometric-dendroclimatological conifer chronologies from Lapland (Scandinavia) and the Alps (Switzerland), *Boreas*, *17*(4), 559–566.
Smerdon, J. E. (2012), Climate models as a test bed for climate reconstruction methods: Pseudoproxy experiments, *WIREs Clim. Change*, *3*, 63–77, doi:10.1002/wcc.149.
von Storch, H., E. Zorita, and F. Gonzáles-Rouco (2009), Assessment of three temperature reconstruction methods in the virtual reality of a climate simulation, *Int. J. Earth Sci.*, *98*, 67–82, doi:10.1007/s00531-008-0349-5.
Wagner, S., and E. Zorita (2005), The influence of volcanic, solar and the Dalton Minimum (1790–1830): CO2 forcing on the temperatures in a model study, *Clim. Dyn.*, *25*(2–3), 205–218.
Wigley, T. M. L., C. M. Ammann, B. D. Santer, and S. C. B. Raper (2005), Effect of climate sensitivity on the response to volcanic forcing, *J. Geophys. Res.*, *110*, D09107, doi:10.1029/2004JD005557.
Wilson, R., R. D'Arrigo, B. Buckley, U. Büntgen, J. Esper, D. Frank, B. Luckman, S. Payette, R. Vose, and D. Youngblut (2007), A matter of divergence: Tracking recent warming at hemispheric scales using tree ring data, *J. Geophys. Res.*, *112*, D17103, doi:10.1029/2006JD008318.